

Calcium spikes accompany cleavage furrow ingression and cell separation during fission yeast cytokinesis

Abhishek Poddar^a, Oumou Sidibe^a, Aniruddha Ray^b, and Qian Chen^{a,*}

^aDepartment of Biological Sciences and ^bDepartment of Physics and Astronomy, University of Toledo, Toledo, OH 43606

ABSTRACT The role of calcium signaling in cytokinesis has long remained ambiguous. Past studies of embryonic cell division discovered that calcium concentration increases transiently at the division plane just before cleavage furrow ingression, suggesting that these calcium transients could trigger contractile ring constriction. However, such calcium transients have only been found in animal embryos and their function remains controversial. We explored cytokinetic calcium transients in the fission yeast *Schizosaccharomyces pombe* by adopting GCaMP, a genetically encoded calcium indicator, to determine the intracellular calcium level of this model organism. We validated GCaMP as a highly sensitive calcium reporter in fission yeast, allowing us to capture calcium transients triggered by osmotic shocks. We identified a correlation between the intracellular calcium level and cell division, consistent with the existence of calcium transients during cytokinesis. Using time-lapse microscopy and quantitative image analysis, we discovered calcium spikes both at the start of cleavage furrow ingression and the end of cell separation. Inhibition of these calcium spikes slowed the furrow ingression and led to frequent lysis of daughter cells. We conclude that like the larger animal embryos, fission yeast triggers calcium transients that may play an important role in cytokinesis (197).

Monitoring Editor

Sophie Martin
University of Lausanne

Received: Sep 28, 2020

Revised: Oct 29, 2020

Accepted: Nov 2, 2020

INTRODUCTION

Calcium is an essential secondary messenger in many cellular processes, but its role during cytokinesis, the last stage of cell division, remains ambiguous. Eukaryotic cells maintain their intracellular calcium at a much lower concentration than that of their extracellular environment. A transient increase in the free calcium level, through either release from the intracellular storage or influx through the

plasma membrane, triggers a number of essential calcium signaling pathways (for a review see Clapham, 2007).

Although the importance of calcium to cytokinesis has long been known (Arnold, 1975), the calcium transients accompanying cytokinesis were discovered much later and remain poorly understood. Fluck *et al.* (1991) first observed two localized calcium waves at the cell division plane of medaka fish embryos during cytokinesis. The first wave initiates just before cleavage furrow ingression, while the second wave appears after cell separation. Follow-up studies discovered similar localized increases of calcium in other animal embryos, including those of zebrafish, *Danio rerio*, and African frogs, *Xenopus laevis* (Miller *et al.*, 1993; Chang and Meng, 1995; Noguchi and Mabuchi, 2002). However, it remains unexplored whether such calcium transients are universal among eukaryotic cells. Neither is there a consensus on the exact molecular function of these transients. The prevailing hypothesis (Fluck *et al.*, 1991; Chang and Meng, 1995) holds that these transients can activate myosin light-chain kinase (MLCK) to promote the activity of the myosin II motor in the contractile ring and trigger ring constriction (Scholey *et al.*, 1980; Craig *et al.*, 1983). This theory draws a parallel between the role of calcium in cytokinesis and that in smooth muscle constriction (Nishimura *et al.*, 1990). This proposal, although attractive, has

This article was published online ahead of print in MBcC in Press (<http://www.molbiolcell.org/cgi/doi/10.1091/mbc.E20-09-0609>) on November 11, 2020.

Author contributions: Q.C. conceptualized the study; Q.C. and A.P. designed and carried out the experiments; Q.C., A.P., O.S., and A.R. analyzed the data; Q.C. and A.P. wrote the manuscript.

*Address correspondence to: Qian Chen (qian.chen3@utoledo.edu).

Abbreviations used: cp-EGFP, circularly permuted enhanced green fluorescent protein; EGTA, ethylene glycol-bis(β-aminoethyl ether)-N,N,N',N'-tetraacetic acid; ER, endoplasmic reticulum; GECI, genetically encoded calcium indicators; MLCK, Myosin light chain kinase; SD, standard deviation; SOCE, store operated calcium release; SPB, spindle pole body.

© 2021 Poddar *et al.* This article is distributed by The American Society for Cell Biology under license from the author(s). Two months after publication it is available to the public under an Attribution–Noncommercial–Share Alike 3.0 Unported Creative Commons License (<http://creativecommons.org/licenses/by-nc-sa/3.0>).

“ASCB®,” “The American Society for Cell Biology®,” and “Molecular Biology of the Cell®” are registered trademarks of The American Society for Cell Biology.

remained unproven even in animal embryos. Adding to the ambiguity, inhibition of the cytokinetic calcium transients in *X. laevis* embryos has produced conflicting results (Miller *et al.*, 1993; Snow and Nuccitelli, 1993; Noguchi and Mabuchi, 2002). To date, both the nature and the molecular function of the cytokinetic calcium transients remain undetermined.

Fission yeast, *Schizosaccharomyces pombe*, has emerged as an excellent model organism for the study of cytokinesis in the last 20 years. The molecular mechanism of cytokinesis in this unicellular organism has been largely conserved in higher eukaryotes (for review see Pollard and Wu, 2010). Like animal cells, fission yeast assembles an actomyosin contractile ring at the cell division plane (Wu *et al.*, 2003), a process mediated by essential cytokinetic proteins such as type-II myosin Myo2p, formin Cdc12p, and cofilin Adf1p (Chang *et al.*, 1997; Balasubramanian *et al.*, 1998; Chen and Pollard, 2011). The assembly of the contractile ring is further promoted by continuous polymerization of actin filaments in the ring (Courtemanche *et al.*, 2016). As in higher eukaryotes, the actomyosin ring constricts to drive cleavage furrow ingression, assisted by a growing septum (Mishra *et al.*, 2013; Laplante *et al.*, 2015). The terminal step of cell separation (for review see Sipiczki, 2007; Garcia Cortes *et al.*, 2016) requires degradation of the septum (Liu *et al.*, 1999; Cortes *et al.*, 2002, 2012; Munoz *et al.*, 2013) as well as proper regulation of the turgor pressure (Proctor *et al.*, 2012; Atilgan *et al.*, 2015).

Although it still remains a challenge to quantify the free calcium concentration in a live cell, the rapid development of genetically encoded calcium indicators (GECI) over the last 20 years has made it far easier than before. Compared to the more widely used synthetic probes, GECIs can be expressed *in vivo* without an intrusive probe-loading procedure. This is particularly advantageous in such genetically modifiable systems as fission yeast. Although most GECIs still trail chemical probes in their sensitivity, some of them, such as GCaMP (Nagai *et al.*, 2001), which we chose for this study, have come close. This single fluorophore sensor consists of three domains: a circularly permuted enhanced green-fluorescent protein (cp-EGFP), a calcium-binding calmodulin motif, and an M13 peptide of human myosin light-chain kinase (MLCK). Binding of calcium to the calmodulin motif dissociates the M13 peptide from cp-EGFP and increases the fluorescence of GCaMP significantly (Nakai *et al.*, 2001). Further modifications of GCaMP have substantially reduced its response time and enhanced its signal-to-noise ratio (Tian *et al.*, 2009; Chen *et al.*, 2013). We picked one of the most sensitive variants, GCaMP6s (Chen *et al.*, 2013), to explore the potential calcium transients during fission yeast cytokinesis.

Few studies have examined the calcium level of fission yeast at the single-cell level, even though its calcium signaling pathways have been characterized extensively. Two central calcium signaling molecules, calmodulin and calcineurin, have been identified (Yoshida *et al.*, 1994; Takeda and Yamamoto, 1987; Moser *et al.*, 1997). As in animal cells, they play a critical role in a plethora of cellular processes in fission yeast, including cytokinesis. In particular, the essential calmodulin Cam1p is required for cell division, underlying the importance of calcium signaling in this model organism (Moser *et al.*, 1997). Past studies have mostly employed bulk assays to determine the average calcium levels of many cells, using either chemical or indirect probes (Deng *et al.*, 2006; Ma *et al.*, 2011). As a result, the regulation of calcium at the cellular level during many processes, including cytokinesis, has been left undetermined.

In this study, we first explored the feasibility of GCaMP-based calcium imaging in fission yeast. We then deployed this probe to capture the calcium transients triggered by various stimuli to validate

its effectiveness. Finally, we identified the cytokinetic calcium spikes and examined their importance to cytokinesis.

RESULTS

Expression and localization of the genetically encoded calcium indicator GCaMP in fission yeast

To probe the intracellular calcium level of fission yeast cells with fluorescence microscopy, we expressed a single copy of the GCaMP coding sequence at an endogenous locus. A strong constitutive ADH promoter drove the expression of GCaMP6s (referred to as GCaMP; Figure 1A). To measure the expression and cellular localization of this calcium indicator, we tagged its C-terminus with another fluorescence protein, mCherry. GCaMP-mCherry localized uniformly throughout the cytoplasm and the nucleus but it was excluded from the vacuoles (Figure 1B). The reporter nevertheless was slightly enriched in the nucleus, as compared with the cytoplasm (ratio = 1.5 ± 0.1 , average \pm S.D., $n = 66$). The intracellular fluorescence of mCherry was uniform in all cells, demonstrating that the calcium indicator GCaMP was expressed homogeneously (Figure 1B). The ratio of GCaMP to mCherry fluorescence also varied very little among these cells (Figure 1C), suggesting that the calcium level of fission yeast cells is mostly constant. We concluded that GCaMP can be expressed homogeneously in the fission yeast cells, and this calcium indicator localizes throughout the intracellular space.

We next determined whether the expression of GCaMP perturbs any cellular functions, a potential concern for endogenously expressed reporters. Overall, the GCaMP-expressing cells exhibited no apparent morphological defects. Their length and width were similar to those of the wild-type cells (Figure 1D). Their mitotic and septation indexes were also normal, similarly to the wild type (Figure 1, E and F). Moreover, these GCaMP-expressing cells did not exhibit any hypersensitivity to either calcium, sorbitol, or EGTA, all of which likely perturb intracellular calcium homeostasis (Supplemental Figure S1). Last, cytokinesis in these GCaMP-expressing cells was unperturbed, as determined by time-lapse fluorescence microscopy. In the GCaMP-expressing cells, the contractile ring assembly and maturation took 44 ± 5 min (average \pm SD; $n = 31$), counted from the appearance of precursor nodes, similarly to the wild-type cells (43 ± 4 min; $n = 40$). This was followed by ring constriction, which took 30 ± 3 min ($n = 43$), identical to that of the wild type (30 ± 3 min; $n = 70$). The last stage of cytokinesis, cell separation, required 26 ± 4 min ($n = 29$) in the GCaMP-expressing cells, not significantly different from the wild type (25 ± 3 min; $n = 67$). These quantitative measurements supported our conclusion that expression of GCaMP does not interfere with cytokinesis either. Because GCaMP does not produce any discernable artifacts, we combined our GCaMP-expressing strain with quantitative microscopy to examine the intracellular calcium level of fission yeast cells.

Calcium transients in fission yeast cells

To validate GCaMP as an effective calcium indicator, we first determined whether an increase in extracellular calcium alters the fluorescence of GCaMP-expressing cells. In the rich YE5s media, addition of 30 mM CaCl_2 increased the average fluorescence of the GCaMP-expressing cells about threefold, as compared with those in YE5s (Figure 2, A and B). The increased extracellular calcium concentration also resulted in more frequent fluctuations of the intracellular GCaMP fluorescence (Figure 2, C and D, and Supplemental Movie S1). Thus, GCaMP-based imaging is fully capable of detecting alterations in calcium concentration.

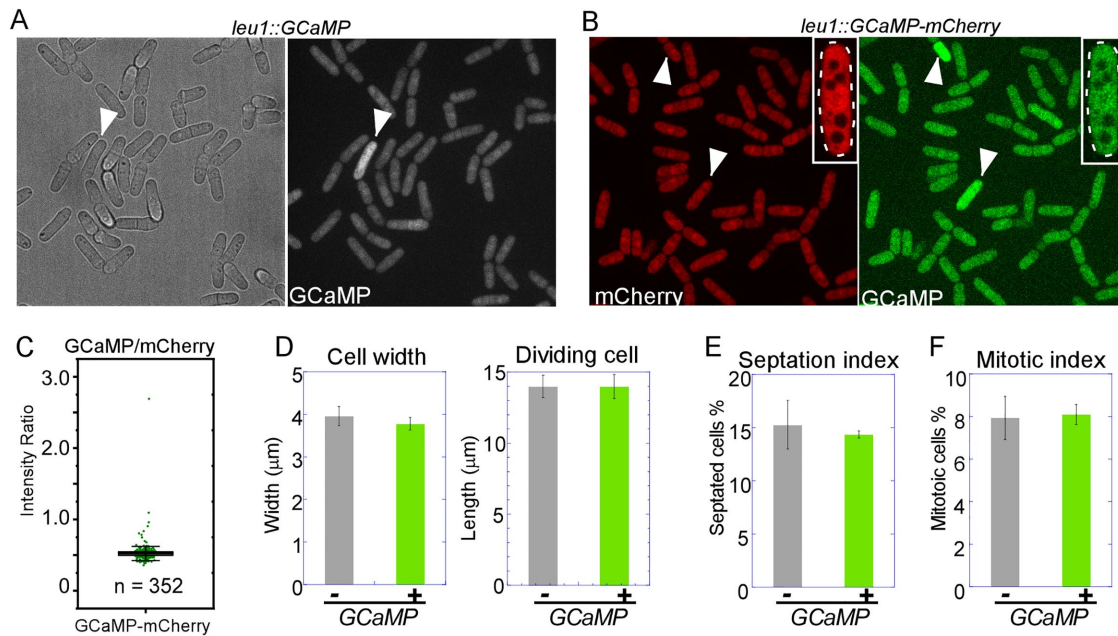


FIGURE 1: Expression and localization of GCaMP in fission yeast. (A) Bright-field (left) and fluorescence (right) micrographs of the cells expressing GCaMP. The intracellular fluorescence was constant for most cells, except for one outlier (white arrowhead). (B, C) Localization and expression of GCaMP-mCherry. (B) Fluorescence micrographs of the cells expressing GCaMP-mCherry. The insert shows the center slice of the Z-series of a representative cell (magnified, outlined in dashed lines). The intracellular fluorescence of mCherry remained low even in two cells with high GCaMP fluorescence (white arrow heads). GCaMP localized throughout the cytoplasm and nucleus, but it was excluded from the vacuoles. Similar results were found in three biological repeats. (C) A box plot showing the ratio of GCaMP:mCherry fluorescence. The intracellular calcium level is homogenous among the cells, resulting in a near-uniform ratio with just a few outliers with likely high calcium level. (D–F) Expression of GCaMP did not produce discernable artifacts. Bars graphs compare the GCaMP-expressing cells to the wild type. (D) The width of all cells (left, $n > 50$) and the length (right, $n > 50$) of dividing cells. No significant differences were found ($p > 0.1$). (E) Septation index ($n > 700$) and (F) mitotic index ($n > 1000$). No significant differences were found ($p > 0.1$). Data are pooled from two biological repeats.

Next, we employed GCaMP-based time-lapse imaging to capture rapid changes in intracellular calcium level, the calcium transients. The untreated fission yeast cells produced only sporadic calcium transients (Figure 2C). We applied various stimuli through microfluidics to produce more transients. First, we used hypoosmotic shock, one of the best-known stimuli for calcium transients in yeast (Batiza *et al.*, 1996; Denis and Cyert, 2002). We found highly synchronized calcium transients in the cells under this shock, captured by an increase in GCaMP fluorescence, (Figure 3A and Supplemental Movie S2). The intracellular calcium rose quickly following the shock and peaked 2 min after the osmotic shock on the average. These calcium transients accompanied the expansion of cell volume closely (Figure 3, B and C). Average amplitude of the calcium increase was proportional to the strength of hypoosmotic shocks (Figure 3D). Second, we applied hyperosmotic shocks to the cells. This, surprisingly, did not elicit detectable calcium transients (Figure 3E and Supplemental Figure S2, A and B). Last, we abruptly increased the extracellular calcium concentration to stimulate the cells. This also provoked strong calcium transients, but they appeared only ~5 min after the infusion of calcium (Figure 3F). As a result of the stimulation, the average intracellular calcium concentration remained elevated after more than 20 min. This response to the external calcium shock confirmed a similar observation made through bulk assays (Deng *et al.*, 2006). Our results demonstrated that GCaMP-based time-lapse imaging can capture calcium transients in fission yeast cells, making it entirely feasible to identify the cytokinetic calcium transients.

Identification of calcium spikes during cytokinesis

As the first step in determining the link between calcium and cytokinesis, we analyzed the intracellular calcium levels in a large number of asynchronized cells. Dividing fission yeast cells can be identified through their increased length. These rod-shaped cells grow by tip extension, starting to grow from a length of ~7 μm after birth. They expand throughout interphase until stopping at a length of ~14 μm at mitotic entry (Mitchison and Nurse, 1985). We found that the calcium level was constant among most cells, regardless of their length ($n = 407$; Figure 4A). However, the calcium concentration of a few cells was significantly higher than the average (>110%). The length distribution of these “outliers” was interestingly bimodal. Two peak fractions are ~14 μm and ~8 μm, respectively (Figure 4B), roughly equaling the lengths of the dividing and newborn cells, respectively. The existence of outlier cells with high calcium levels provided the first hint of calcium transients during cell division.

Next, we examined the temporal regulation of intracellular calcium in the dividing cells through time-lapse microscopy. To facilitate our analysis, these cells expressed both GCaMP and well-established fluorescence protein markers of cytokinesis. First, we looked closely at the calcium level during mitosis by imaging the cells expressing both GCaMP and Sad1p-GFP, a marker of spindle pole bodies (SPBs). In fission yeast, the separation of SPBs is concomitant with the start of prometaphase, followed by anaphase, which ends in ~30 mins (Supplemental Figure S3A; Wu *et al.*, 2003). During this period, we captured very few calcium transients. About 30 min after the separation of SPBs, the calcium level started to rise significantly throughout the intracellular space and peaked at 34 min

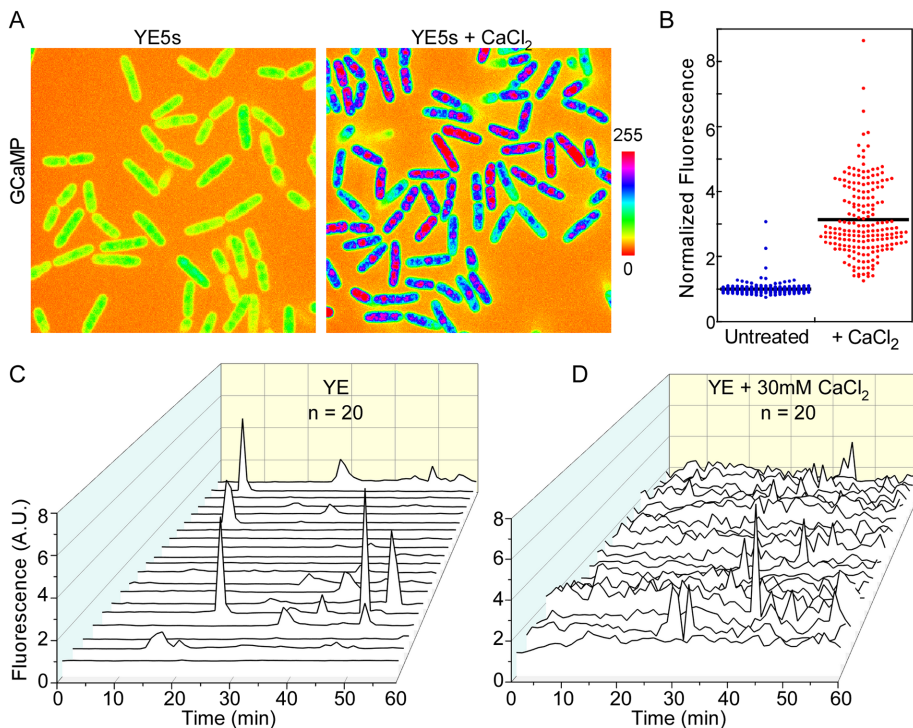


FIGURE 2: GCaMP responds to the intracellular calcium level increase. (A, B) The intracellular GCaMP fluorescence increased with added calcium in the media. The micrograph and measurements were acquired about 5–10 min after addition of 30 mM CaCl₂, likely after the intracellular calcium level has reached an equilibrium. (A) Fluorescence micrographs (spectrum colored) of the GCaMP-expressing cells in either YE5s (left) or YE5s supplemented with 30 mM CaCl₂ (right). Bar represents the intensity scale. (B) Dot plot of fluorescence intensities of the cells ($n > 190$). Black line represents the average. Added calcium increased the average intracellular fluorescence \sim threefold ($p < 0.001$). (C, D) Calcium homeostasis of fission yeast cells. 3D line plots show the time courses of intracellular GCaMP fluorescence in either YE5s, C, or YE5s plus 30 mM CaCl₂, D. The time-lapse movies were recorded at a frequency of 1 frame/min. Increased calcium in the media resulted in more frequent fluctuations of the intracellular calcium level. Time zero represents the start of the time-lapse microscopy, \sim 10 min after the addition of calcium. Data are pooled from two biological repeats.

(Supplemental Figure S3C), which we termed calcium spikes. These spikes appeared to be well synchronized, coinciding with telophase as well as early cytokinesis (Supplemental Figure S3, B and C). Next, we determined whether these calcium spikes initiated exactly at the beginning of furrow ingression, as calcium transients did in fish embryos (Fluck *et al.*, 1991; Chang and Meng, 1995). We imaged the cells' expressed GCaMP and a contractile ring marker Rlc1p-tdTomato, the regulatory myosin light chain (Figure 5A). Our movies recorded very few calcium spikes during the assembly and maturation of the contractile ring (Figure 5, A and B). In comparison, the time-lapse microscopy captured calcium spikes accompanying the start of ring constriction in most dividing cells (90%, $n = 62$), despite a limited sampling rate of one frame every 2 min. We called these "constriction spikes" (Figure 5, B and C, and Supplemental Movie S3). Additional spikes also appeared throughout the ring constriction. In these cytokinetic cells, the average intracellular calcium level reached a peak \sim 1.9-fold over the baseline ($p < 0.001$) within 1 ± 3 min (average \pm SD; $n = 64$) of the start of the cleavage furrow ingression (Figure 5D).

Besides the dividing cells, the newborn cells as well appeared to have high intracellular calcium, prompting us to examine the calcium spikes during cell separation. Although few calcium spikes were captured following the ring closure and before the cell separa-

tion, spikes were found in most cells (84%, $n = 73$) immediately after the separation (Figure 6A). Compared with the constriction spikes, these separation calcium spikes appeared to be more synchronous. This is likely due to more precise alignment of the time courses based on the cell separation than based on the start of contractile ring constriction. These separation spikes were concomitant with the initial appearance of new ends. They distributed asymmetrically between the two daughter cells (Figure 6, B and C). Among the cells in which at least one separation spike was captured, 52% triggered a calcium spike in only one daughter cell. The other 48% triggered spikes in both daughter cells, one closely following the other (Figure 6, B and C). On the average, the separation spikes increased the intracellular GCaMP fluorescence \sim 1.8-fold ($n = 44$; Figure 6, D and E). The calcium level peaked \sim 2 min after the end of cell separation ($p < 0.001$; Supplemental Movie S4). We observed similar constriction and separation spikes in the dividing cells inoculated in the synthetic EMM5s media (Supplemental Figure S3, D and E), further confirming the existence of these cytokinetic spikes.

To better understand the spatiotemporal regulation of these cytokinetic calcium spikes, we characterized them by fast imaging. We increased the frequency of time-lapse acquisition 40-fold, from one frame every 2 min to one frame every 3 s. We captured only a limited number of constriction and separation spikes in this way (Figure 7, A and D). Close examination of the spikes found that they increased the intracellular calcium level heterogeneously throughout cytoplasm (Figure 7, B and E). They exhibited a lifespan of $50^{\circ}200$ s and their amplitudes were highly variable (Figure 7, C and F). Some constriction spikes exhibited a more than 10-fold increase in GCaMP fluorescence above the baseline level (Figure 7C). We concluded that the cytokinetic calcium spikes rise throughout the cytoplasm and are highly heterogeneous.

Functions of cytokinetic calcium spikes

The close temporal correlation between calcium spikes and cytokinesis prompted us to investigate whether these spikes are required for cytokinesis. To this end, we depleted the extracellular calcium from the media, hypothesizing that the calcium influx contributes to the spikes. The calcium depletion was only temporary to minimize the effects on other calcium-dependent processes. The cells were observed in either EMM5s media without any supplemented calcium or YE5s media supplemented with low concentrations (1–2 mM) of EGTA. At such concentrations, we found that EGTA did not inhibit cell growth strongly (Supplemental Figure S4A). In the calcium-depleted media, the average intracellular GCaMP fluorescence remained unchanged in YE5s plus 1 mM EGTA, but decreased significantly in either 2 mM EGTA (13%) or the calcium-free EMM5s media (12%; Figure 8, A and B). Nevertheless, the fraction of outlier cells that exhibited elevated calcium levels decreased

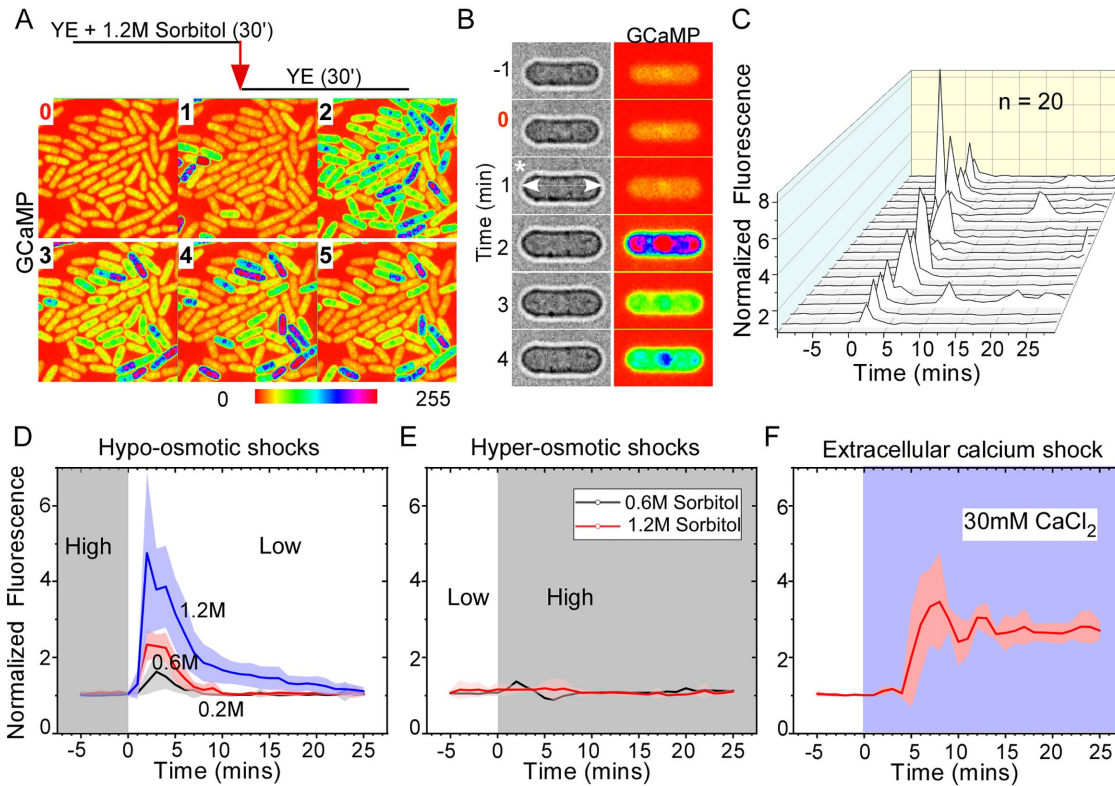


FIGURE 3: Osmotic shocks trigger calcium transients. (A–C) Hypoosmotic shock triggered calcium transients in fission yeast cells. The GCaMP-expressing cells, trapped in a microfluidic chamber, were first equilibrated in YE5s supplemented with 1.2 M sorbitol for 30 min before the infusion of YE5s without sorbitol (time zero). (A) Time-lapse micrographs (spectrum-colored) of a representative field in the chamber. The hypoosmotic shock triggered a synchronized calcium spike in the cells. (B) Time-lapse micrographs of a representative cell. In the media with 1.2 M sorbitol, the cell appeared shrunk. After the shock (time zero), the cell expanded quickly (asterisk), followed by calcium transient (right, spectrum-colored). Number: time in minutes. (C) 3D line plots of the time courses of GCaMP fluorescence in 20 representative cells. The shock triggered synchronized calcium transients in every cell. Representative results from three biological repeats are shown. (D–F) Average time courses of the intracellular GCaMP fluorescence during either hypoosmotic, D, or hyperosmotic, E, or extracellular calcium, F, shocks applied through microfluidics. The clouds represent standard deviations. These stimuli triggered distinct change of intracellular calcium level. (D) The cells were first equilibrated in YE5s with various concentrations of sorbitol for 30 min before the infusion of YE5s media (time zero). The amplitudes of calcium transients increased significantly ($p < 0.001$) as the strength of shocks increased. The p values are derived from comparing the peak values of average GCaMP fluorescence during shocks. (E) The cells were first equilibrated in YE5s media for 30 min before the infusion of YE5s media supplemented with various concentrations of sorbitol (time zero). No significant change of calcium was triggered by hyperosmotic shock. (F) The cells were equilibrated in YE5s media for 30 min before the infusion of YE5s plus 30 mM CaCl_2 (time zero). The addition of extracellular calcium triggered a delayed intracellular calcium increase. Data are pooled from three biological repeats.

substantially under all three conditions (Figure 8, A and B). Although the calcium spikes were no longer as visible under these conditions, quantitative image analysis revealed that the average number of cytokinetic spikes in each cell was not reduced but the amplitude of these spikes decreased dramatically (Figure 8, C–F; Supplemental Figure S4, B–E). We concluded that the cytokinetic calcium spikes can be inhibited by depleting extracellular calcium from the media.

We next examined cytokinesis in the cells whose calcium spikes were inhibited. Through time-lapse microscopy, we found that the assembly and maturation of the contractile ring took a slightly longer time (11%) in the calcium-free EMM media than in the EMM media (Figure 9, A and C). However, constriction of the contractile ring slowed much more dramatically (30%; Figure 9E and Supplemental Movie S5). EGTA (1 or 2 mM) did not delay the assembly and maturation of the ring significantly (Figure 9, B and D) but it inhibited the ring constriction significantly in a dosage-dependent man-

ner. The rate was down ~50% in YE5s plus 2 mM EGTA, compared with YE5s (Figure 9E). When EGTA concentration was further increased to 5 mM, most contractile rings (90%; $n = 30$) disintegrated without completing the constriction (Supplemental Figure S5, A and B). We also examined the cell separation when the calcium spikes were inhibited. Surprisingly, the duration of cell separation remained normal when the extracellular calcium was depleted (Supplemental Figure S5, C and D). Although no daughter cells lysed in the calcium-free EMM5s media, 2 mM EGTA induced more than one-third of the daughter cells to lyse ($35 \pm 5\%$; $n = 103$) following the separation (Figure 9, G and H). More cells lysed when the concentration of EGTA increased to 5 mM (unpublished data). Pmr1p is an ER calcium ATPase that replenishes the internal storage of calcium (Cortes et al., 2004). As expected, depletion of intracellular calcium by deleting *pmr1* resulted in frequent lysis of daughter cells in the calcium-free EMM5s media ($38 \pm 9\%$; $n = 60$), even though very few mutant cells lysed in the regular EMM5s ($3 \pm 4\%$; $n = 47$). We

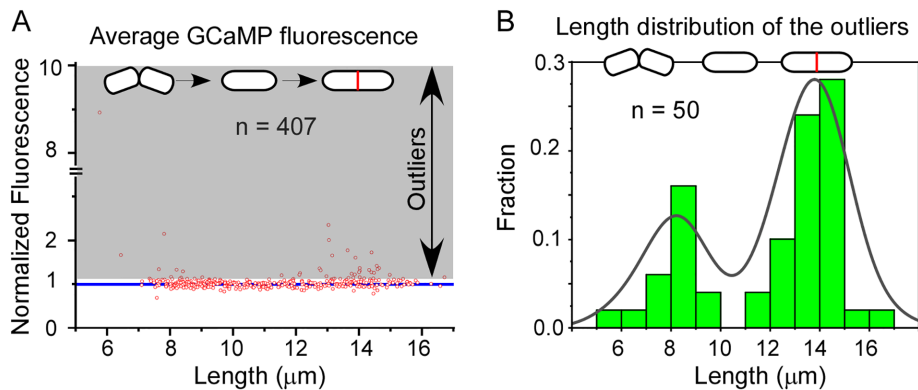


FIGURE 4: Correlation between intracellular calcium level and cell division. The intracellular calcium level in asynchronous cells, based on the GCaMP fluorescence. Top: cartoon representations of fission yeast cells at birth, growth, and division. (A) A scatterplot showing the relationship between the intracellular calcium level and the cell length. The calcium level of most cells was uniform (blue line). Only a few outlier cells (50/407) exhibited elevated calcium level (shaded area > 110% of the average). (B) A histogram showing the distribution of the cell length among the outliers. The black line represents the best fit of a bimodal distribution. Two peak fractions represent the cells of 8–9 μm and those of 14–15 μm , roughly corresponding to newborn and dividing cells, respectively. The data are pooled from four biological repeats.

concluded that calcium promotes contractile ring constriction as well as the integrity of separating cells, likely through cytokinetic calcium spikes.

DISCUSSION

Overall, we demonstrated that GCaMP-based imaging allows fission yeast to serve as a powerful model organism for the study of calcium transients during various cellular processes. Using this method, we discovered cytokinetic calcium spikes in this unicellular model organism for the first time. These calcium transients are similar to those first uncovered in animal embryos. Calcium likely plays a critical role in promoting ring constriction and daughter cell integrity through these transients.

GCaMP-based calcium imaging of fission yeast

To our knowledge, our study is the first to examine the feasibility of GCaMP-based calcium imaging in fission yeast cells. We are fortunate that fission yeast is quite tolerant of the expression of this calcium indicator. It does not perturb many cellular processes that we examined, even when it is expressed constitutively. More importantly, GCaMP is also highly sensitive as a probe for time-lapse microscopy, allowing us to capture calcium transients at a relatively low sampling rate. Compared with synthetic calcium probes, GCaMP exhibited two key advantages in fission yeast. First, unlike synthetic probes such as Calcium Green (Chang and Meng, 1995), GCaMP can be maintained at a constant intracellular concentration through the homogenous expression of this reporter. Combined with quantitative microscopy, this largely eliminated the heterogeneity of fluorescence intensities among cells. In contrast, the intracellular concentration of the synthetic probes can be highly variable among cells. This advantage of GCaMP was exemplified by the identification of outliers with high calcium concentration among a large number of cells. The other advantage of GCaMP is its more uniform cellular distribution, as compared with the synthetic probes. This allows detection of calcium transients throughout the cytoplasm as well as the nucleus.

When combined with yeast genetics, GCaMP can be a very versatile tool for studying calcium signaling. As an example, we con-

structed both GCaMP and GCaMP-mCherry, both of which have potential to be employed in the future studies. We employed GCaMP, not GCaMP-mCherry, throughout this study, primarily to preserve the spectrum for imaging the fluorescence protein markers of cytokinesis. Nevertheless, the tandem reporter can be used for ratiometric imaging of intracellular calcium, potentially providing a higher signal-to-noise ratio. Overall, application of GCaMP will make fission yeast an attractive model organism for studying calcium transients and homeostasis in nonexcitable cells.

Evolutional conservation of the cytokinetic calcium transients

Our study provides fresh evidence for the existence of calcium transients in a unicellular organism. Similarly to the earlier studies (Fluck *et al.*, 1991; Chang and Meng, 1995; Noguchi and Mabuchi, 2002), we employed live fluorescence microscopy to determine the temporal correlation between the calcium transients and cytokinesis. With the availability of fluorescence protein markers of cytokinesis, we now determined the temporal regulation of these spikes with more precision. In addition to time-lapse microscopy, we sought out an alternative approach to illustrate this close correlation. We analyzed just snapshots of many GCaMP-expressing cells to reveal the relationship between cell division and intracellular calcium level. Compared with the movies, the snapshots examined all cells regardless of their cell-cycle stage, presenting a less biased view of the potential calcium change in them. Combined with the previous studies of animal embryos, our results strongly support the conclusion that a temporal increase of calcium during cytokinesis may be evolutionally conserved.

The temporal regulation of fission yeast cytokinetic calcium spikes bears strong similarities to that found in the animal embryos. The constriction spikes of fission yeast are comparable to the first “furling wave” observed in the animal embryos (Fluck *et al.*, 1991), which initiates just as the cleavage furrow starts to ingress (Chang and Meng, 1995; Noguchi and Mabuchi, 2002). The separation spikes are comparable to the second “zipping wave” of the embryos, which starts just when the two daughter cells separate (Fluck *et al.*, 1991; Noguchi and Mabuchi, 2002). Both the calcium waves in the embryos and the spikes in fission yeast can last for minutes, far longer than other known calcium transients (Jaffe and Creton, 1998). Although no calcium spikes have been identified yet during budding yeast cytokinesis, Carbo *et al.* (2017) observed higher frequency of calcium bursts during G1 to S phase transition in synchronized cells, which may be similar to the separation calcium spikes in fission yeast. Overall, our study suggests that the regulatory mechanism of calcium during cytokinesis may have been conserved as well.

There are also key differences between the calcium spikes and these embryonic calcium waves. Chief among them is the spatial regulation of these calcium transients. In fission yeast, the calcium spikes propagate globally throughout the cytoplasm and nucleus. In contrast, the calcium waves of animal embryos are restricted to the cleavage furrow (Fluck *et al.*, 1991; Chang and Meng, 1995) or its surrounding region (Noguchi and Mabuchi, 2002). Although this

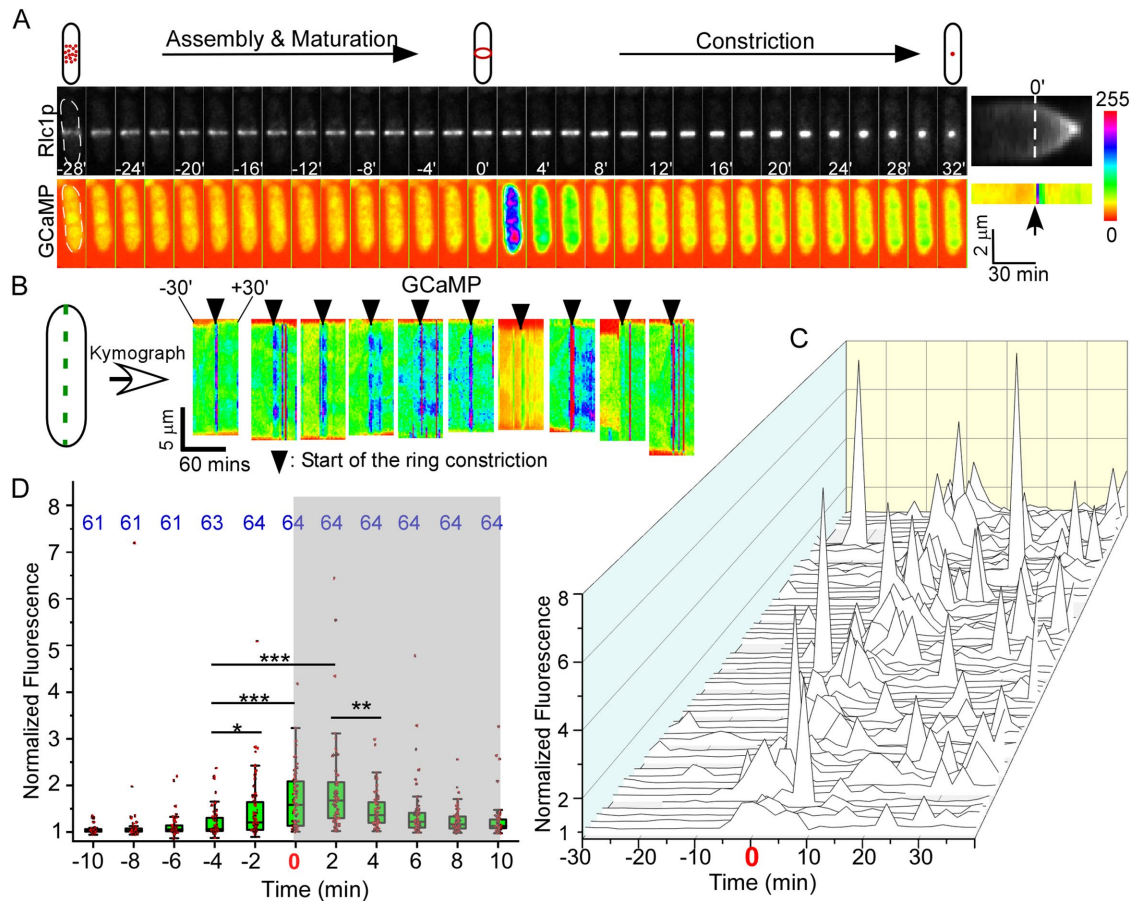


FIGURE 5: Calcium spikes accompany the cleavage furrow ingression. (A, B) The calcium spikes accompanied the contractile ring constriction. (A) Left: Time-lapse micrographs of a dividing cell expressing both Rlc1p-tdTomato (gray, top) and GCaMP (spectrum-colored, bottom). Number: time in minutes after the start of ring constriction. Interval = 2 min. Right: Kymograph of the contractile ring (top) and the GCaMP fluorescence, with the dashed lines marking the start of ring constriction. A calcium spike initiated at time zero and peaked at +2 min. Bar represents the relative scale of the intracellular calcium level. (B) Kymographs of GCaMP fluorescence in 10 representative cells from -30 min to +30 min, relative to the initiation of ring constriction. (C, D) Quantitative analysis of the intracellular calcium level during the ring constriction. Data are pooled from three biological repeats. (C) 3D line plots showing the time courses of calcium level in representative cells ($n = 64$). (D) Boxplots of intracellular calcium level in the cells shown in C. The number on top indicates the number of observations made at each time point. The average intracellular calcium level increased significantly starting at -2 min and peaked at +2 mi (1.9 ± 1.0 , average \pm SD), relative to the baseline average. * $p < 0.05$. ** $p < 0.01$. *** $p < 0.001$.

difference may be due to a difference in sensitivity of the calcium probes, we propose that this distinction is likely due to the relatively small size of fission yeast cells, measuring only $4 \mu\text{m}$ wide and $14 \mu\text{m}$ long, compared with embryos of hundreds of micrometers. So far, we have found no evidence that the constriction spike of fission yeast triggers contractile ring constriction, even though there is evidence that the furrowing waves trigger the ring constriction (Fluck *et al.*, 1991; Miller *et al.*, 1993; Chang and Meng, 1995). Last, the asymmetry of the separation spikes is also unique to fission yeast. It may be linked to the asymmetric turgor pressure in the two daughter cells during separation.

Mechanism of the calcium spikes and their potential roles

Although the regulatory mechanism for these cytokinetic calcium spikes remains to be explored, our data suggest that they likely draw calcium from both the influx and internal release. Inhibition of the influx through depleting extracellular calcium inhibited the spikes significantly but not completely. Under this condition, the

cytokinetic calcium spikes still occurred, albeit with greatly diminished amplitude. This points to ER- or vacuole-stored calcium as the other likely source for the spikes. Supporting this hypothesis is our observation that EGTA exhibited a stronger inhibitory effect on cytokinesis, compared with the calcium-free EMM medium. EGTA may have chelated the intracellular calcium slowly during long-term incubation. This is consistent with the frequent lysis of *pmr1Δ* mutant during the cell separation in the calcium-free medium. In comparison, the embryonic calcium waves draw only from the internal store (Miller *et al.*, 1993; Chang and Meng, 1995). It remains unclear what are the ion channels mediating the cytokinetic calcium transients. Fluck *et al.* (1991) first proposed the potential role of tension-sensing calcium channels, which can be activated during cytokinesis. This remains a feasible mechanism, considering increased membrane tension on the cleavage furrow. On the other hand, release of internal calcium could be through the store-operated calcium release (SOCE) channels (Chan *et al.*, 2015, 2016). Nevertheless, none of these cytokinetic ion channels have been identified.

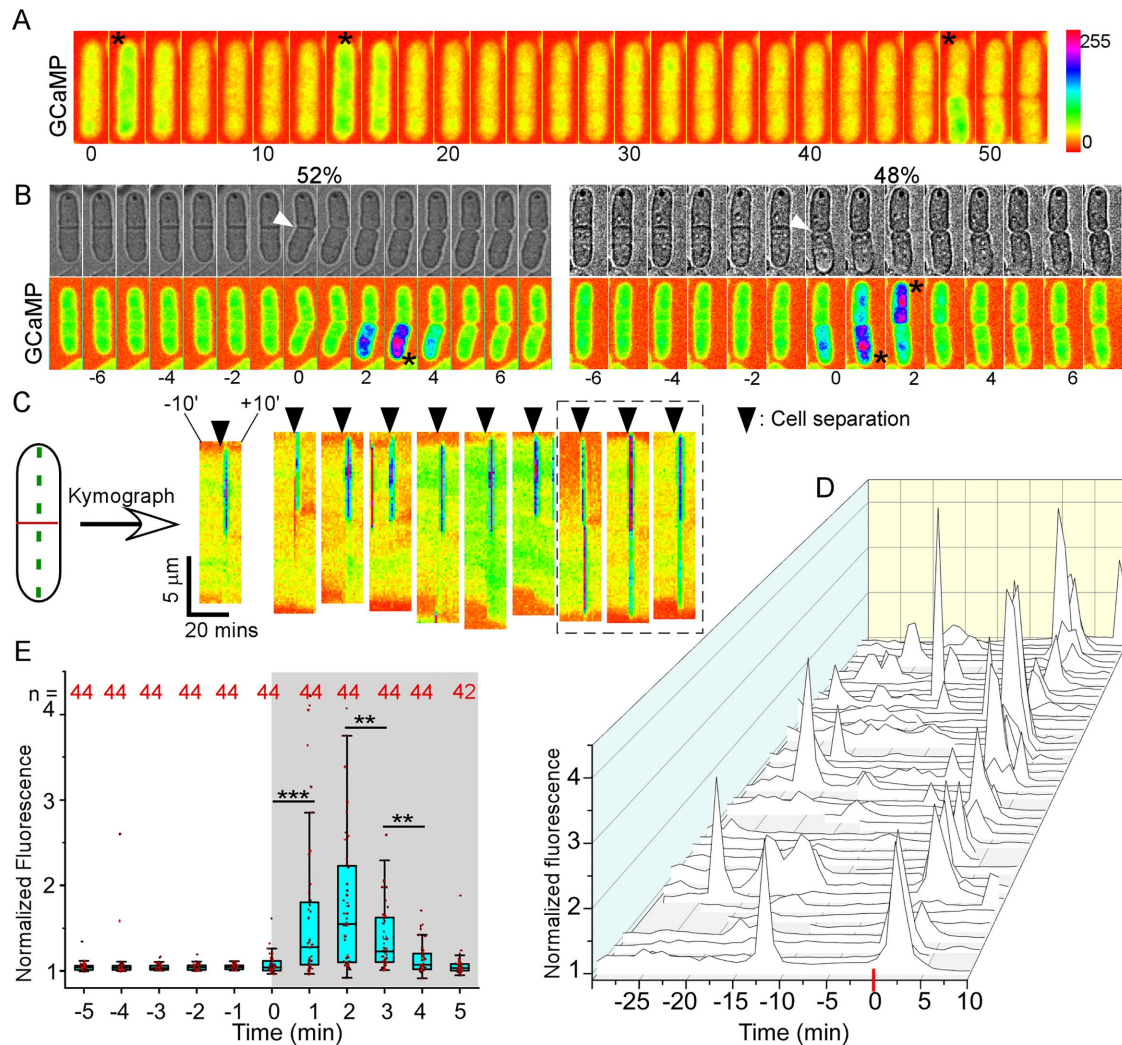


FIGURE 6: Calcium spikes accompany cell separation. (A–C) Cytokinetic calcium spikes during cell separation (white arrowhead). Asterisk: the peak of a spike. Bar: the relative scale of intracellular calcium level. (A) Time-lapse micrographs of a cell expressing both GCaMP (spectrum-colored) and Rlc1p-tdTomato (unpublished data). Three calcium spikes (asterisk) are detected in this cell, including one following the start of ring constriction (time zero), the second during the ring constriction, and the third after cell separation (arrowhead). Number: time in minutes. Interval = 2 min. (B) Time-lapse micrographs of two cells expressing GCaMP (bottom). Interval = 1 min. Number: time in minutes after cell separation (time zero, arrowhead). The spikes appeared either in just one daughter cell (top) or separately in both daughter cells (bottom). Arrowhead: completion of the cell separation. (C) Kymograph of separation spikes in 10 representative cells. Dashed box: the asymmetric separation spikes in both daughter cells. (D, E) Quantification of the intracellular calcium level during the separation. The time-lapse movie was captured at a frequency of 1 frame/min. The data are pooled from four biological repeats. (D) 3D line plots showing the time courses of intracellular calcium level in the dividing cells ($n = 44$). A highly synchronized calcium spike followed the cell separation (time zero) in most cells. (E) Boxplots of the calcium level of the cells shown in D. The number of observations at each time point is indicated on the top. The average calcium level started to increase at 0 min and peaked at +2 min (1.8 ± 0.8 , average \pm SD). $** p < 0.01$. $*** p < 0.001$.

Although our study clearly showed that calcium is important for fission yeast cytokinesis, it leaves unanswered whether this is exclusively through the calcium spikes. This is in part due to the technical difficulty of separating the function of the spikes from that of the intracellular calcium level. Our method of depleting extracellular calcium led to both inhibition of calcium spikes and a slight drop of intracellular calcium level. Although we favor the model that these spikes can regulate cytokinesis, our current results cannot rule out the possibility that a threshold level of intracellular calcium is sufficient for cytokinesis. From comparing the inhibition of cytokinesis by 1 and 2 mM EGTA, it is likely that both the spikes

and the intracellular calcium level contribute to cytokinesis. Nevertheless, both the constriction and separation spikes likely activate the calcium signaling pathways during cytokinesis. The constriction spikes may increase the activity of type II myosin in the ring through the phosphorylation of myosin regulatory light chain (Fluck *et al.*, 1991; Chang and Meng, 1995). Alternatively, the transient increase of calcium could stimulate the septum biosynthesis through activating the calcium-dependent calcineurin (Yoshida *et al.*, 1994; Cadou *et al.*, 2013; Martin-Garcia *et al.*, 2018). The separation spikes could result from a drop in turgor pressure in the daughter cells following the separation, similar to those triggered by

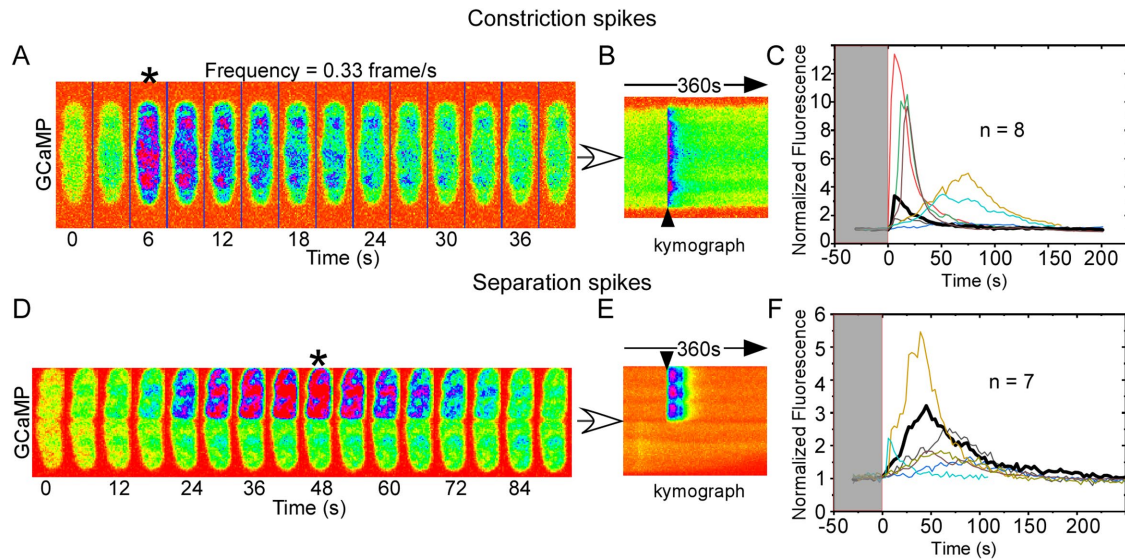


FIGURE 7: Spatiotemporal regulation of cytokinetic calcium spikes. The spikes were captured at a frequency of one frame every 3 s during the time-lapse microscopy. Representative constriction, A–C, or separation spikes, D–F, are shown. (A, D) Time-lapse micrographs (spectrum-colored) of two GCaMP-expressing cells during cytokinesis. Arrowhead: hot spot of calcium increase in the cytoplasm. Number: time in seconds after the initial rise of calcium (Time zero). Asterisk: the peak of calcium level. (B, E) Fluorescence kymograph of the spikes. Calcium increased heterogeneously throughout the intracellular space during the spikes. (C, F) Time course of cytokinetic spikes, including the one shown on the left (thick black line). The cytokinetic calcium spikes are highly heterogeneous, with various amplitudes and lifespans. Data are pooled from three biological repeats.

hyposmotic stress. Alternatively, these spikes may modulate the turgor pressure throughout the cell separation (Proctor *et al.*, 2012; Abenza *et al.*, 2015). Further studies will be required to determine the downstream targets of cytokinetic calcium spikes.

EXPERIMENTAL PROCEDURES

Yeast genetics

We followed the standard protocols for yeast cell culture and genetics. Tetrads were dissected with a Spore+ micromanipulator (Singer, UK). Yeast cells were transformed by the lithium acetate method. The *pmr1Δ* mutant is from a commercially available fission yeast deletion library (Bioneer, South Korea). All the strains used in this study are listed in Supplemental Table S1.

To construct the GCaMP-expressing strain, we amplified the coding sequence from *pCMV-GCaMP6s* (Addgene, Plasmid #40753) through PCR using primers P589 and P590. The DNA fragment was subcloned into a previously described plasmid *pFA6a-KanMX6-Padh1-Tadh1* (Chen and Pollard, 2013). The GCaMP6s ORF, together with the *Adh1* promoter and terminator, was integrated into the *leu1* locus through PCR-based homologous recombination using primers P413 and P414 (Bahler *et al.*, 1998). The resulting strain was confirmed through both PCR using primers P589 and P416 and Sanger sequencing using primer P668. The GCaMP-mCherry strain was constructed through homology-based PCR using primers P647 and P648. The genome locus was sequenced to confirm the insertion of mCherry coding sequence. All the primers used in this study are listed in Supplemental Table S2.

Fluorescence microscopy

For time-lapse microscopy, the cells were first inoculated in liquid YE5s media at 25°C for 2 days before being harvested during the exponential growth phase at a density between 5×10^6 /ml and 1.0×10^7 /ml. A sample of 20 μ l of the cell culture was spotted onto a glass coverslip (#1.5) in a 10-mm Petri dish (Cellvis, USA). The

coverslip was precoated with 50 μ l of 50–100 μ g/ml lectin (Sigma, L2380) and allowed to dry for 3–4 h in a 30°C incubator. After 10 min at room temperature, most cells attached to the coverslip in the Petri dish. YE5s medium (2 ml) was then added to the dish before microscopy. When chelation of calcium in medium is required, 2 ml of YE5s supplemented with EGTA was added instead.

For the experiments in the calcium-free media, we prepared the synthetic EMM media by omitting CaCl_2 (100 μ M) and replacing calcium pantothenate (Vitamin B5) with sodium pantothenate (Cayman Chemical, Cat# NC1435671). The cells were first inoculated in YE5s medium for 1 day, followed by another ~15 h in EMM5s. After harvesting the exponentially growing cells, we washed them three times with the calcium-free media before proceeding to microscopy.

We employed a spinning-disk confocal microscope for the time-lapse microscopy. The microscope is an Olympus IX71 unit equipped with a CSU-X1 spinning-disk unit (Yokogawa, Japan). The motorized stage (ASI, USA) includes a Piezo Z Top plate for acquiring Z-series. The images were captured on an EMCCD camera (IXON-897, Andor) controlled by iQ3.0 (Andor). Solid-state lasers of 488 and 561 nm were used in the fluorescence microscopy, at a power of no more than 2.5 mW. Unless specified, we used a 60 \times objective lens (Olympus, Plan Apochromat, NA = 1.40). Typically, a Z-series of eight slices at an interval of 1 μ m was captured at each time point during the time-lapse microscopy. The temperature was maintained at $-22 \pm 2^\circ\text{C}$ in a designated room for microscopy. To further minimize environmental variations, we typically imaged both control and experimental groups in randomized order on the same day.

For visualization of septum, we fixed the cells with 4% formaldehyde (EMS, USA) before staining them with 1 μ g/ml calcofluor white (Sigma, Cat# 18909). For visualization of nuclei, we fixed the cells with 70% cold ethanol before staining them with 1 μ g/ml DAPI

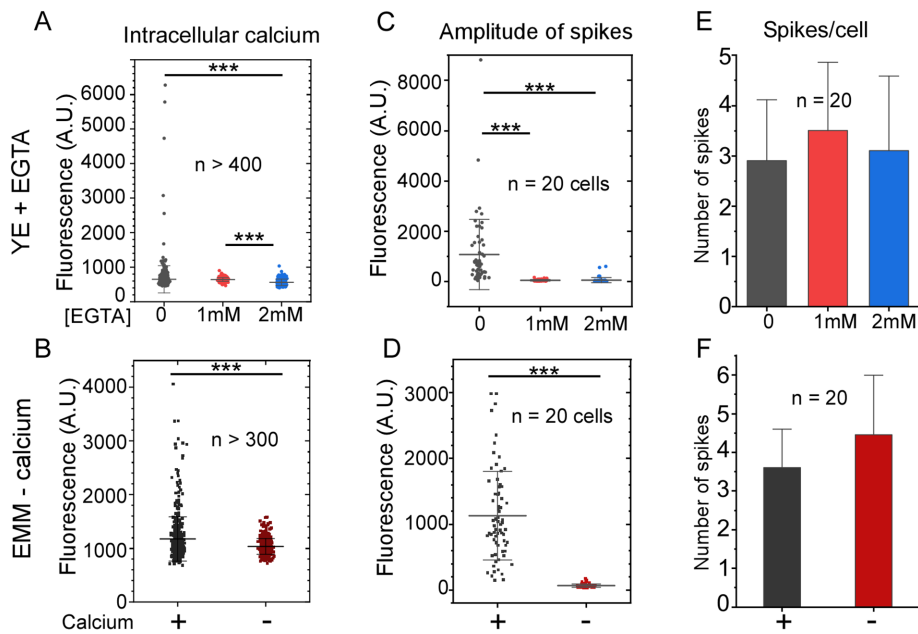


FIGURE 8: Depletion of extracellular calcium inhibits the cytokinetic calcium spikes. Either supplementation of EGTA or removal of calcium from the media inhibited the calcium spikes. (A, B) Dot plots overlaid with average \pm SD showing the intracellular calcium level. Although 1 mM EGTA did not change the average intracellular calcium level significantly ($p > 0.05$), 2 mM EGTA and the calcium-free EMM5s media reduced it significantly, by 13% and 12% respectively. All three conditions greatly reduced the number of outliers which exhibited high calcium level. (C–F) Bar graphs showing amplitude of calcium spikes, C and D, and number of spikes per cell, E and F, in 20 representative cells from -10 to $+60$ min, relative to the start of contractile ring constriction. The amplitude and number of these spikes are quantified through computer-assisted thresholding as described in *Materials and Methods*. Depletion of extracellular calcium reduced the average amplitude of calcium spikes significantly, but not the number of spikes per cell. $***p < 0.001$. Data are pooled from two biological repeats.

(Roche, Cat# 1023627001). To image fixed cells, we used an Olympus IX81 microscope equipped with a XM10 camera and a mercury lamp.

To apply osmotic and calcium stresses, we used a CellASIC ONIX2 system (EMD Millipore) controlled by a desktop computer through the software ONIX (EMD Millipore). To trap cells in the imaging chamber of a microfluidics plate (Y04C), we injected the exponentially growing cell culture into the chamber at a pressure of 34.5 kPa for 2 min, followed by a continuous infusion of YE5s media at a pressure of 10 kPa for another 30 min. To apply hyperosmotic stresses, we injected YE5s plus sorbitol into the chamber at a pressure of 10 kPa. Similarly, to apply hypo-osmotic stresses, we injected YE5s into the chamber at a pressure of 10 kPa after the chamber had been equilibrated with a continuous infusion of YE5s plus sorbitol for 30 min.

We captured the kinetics of cytokinetic calcium spikes by time-lapse microscopy of the GCaMP-expressing cells at a frequency of 0.33 frames/s without the Z-series. A complete spike is defined as one with a single peak rising from and decaying to the baseline level. For the constriction spikes, we examined the dividing cells with either two separating nuclei or a constricting ring.

Image processing and analysis

We quantified the intracellular fluorescence of a GCaMP-expressing cell as the total fluorescence intensity of the cell divided by its area. This value was used to represent the intracellular calcium level throughout the study. Cells were segmented manually, and their

fluorescence intensities were quantified using average intensity projections of the Z-series. The intracellular fluorescence of the cells trapped in a microfluidics chamber was quantified by subtracting the background fluorescence of the camera from their combined fluorescence. Unless specified, we normalized the intracellular fluorescence of a cell against the baseline value, which is typically defined as the average of the five lowest values recorded during a time course. The microscopy images acquired during osmotic or calcium shocks were analyzed by quantifying two regions of interest in cytoplasm, each measuring $1 \mu\text{m}$ in diameter. The statistics tests were done using Excel. In most cases, the two-tailed Student's *t* test was used. Standard deviations (SD) are used throughout the study to represent data deviations.

To manually quantify the fraction of cells with either constriction or separation spikes, we defined a spike as a fluorescence increase of more than four times the SD over the baseline value before the spike. For the constriction spikes, we calculated the prespike average (baseline) and SD based on the intracellular fluorescence of a dividing cell from -34 to -6 min, relative to the start of the contractile ring constriction. A constriction spike will be found within a time window of -4 to $+6$ min. For the separation spikes, we calculated the prespike average (baseline) and SD based on the intracellular fluorescence of a separating cell from -11 to -1 min, relative to the end of cell separation. A separation spike will be found within a time window of between 0 and $+4$ min.

For computer-assisted quantification of the amplitudes and number of cytokinetic calcium spikes in Figure 8, we used thresholding through a custom-written algorithm. These 2 min-interval videos (from -10 to $+60$ min, relative to the start of the contractile ring constriction) of dividing cells are first preprocessed using a median filter to reduce noise. This nonlinear filter helps smooth the images while preserving high spatiotemporal resolution. Following the noise removal, the background fluorescence signal from the cells is eliminated by subtracting the temporal average of each pixel in every frame. This process enables us to retain most of the flickering events, while eliminating the background fluorescence to a large extent. The average fluorescence intensity of a cell is then calculated by applying a binary mask on the images. Binarization of the median filtered images is performed using Otsu's thresholding method and applied to the background subtracted images. The average fluorescence intensity value at each time point is then recorded and used for analysis. Prior to identifying the peaks, we perform a temporal averaging of the signal, using two consecutive time points, to eliminate the small fluctuations within the data. Further thresholding of the signal is performed by nullifying the values lower than the temporal average of the entire signal. The temporal average is used as one of the criteria to distinguish the peaks from background fluctuations. This thresholding step removes the variation in the remnant background

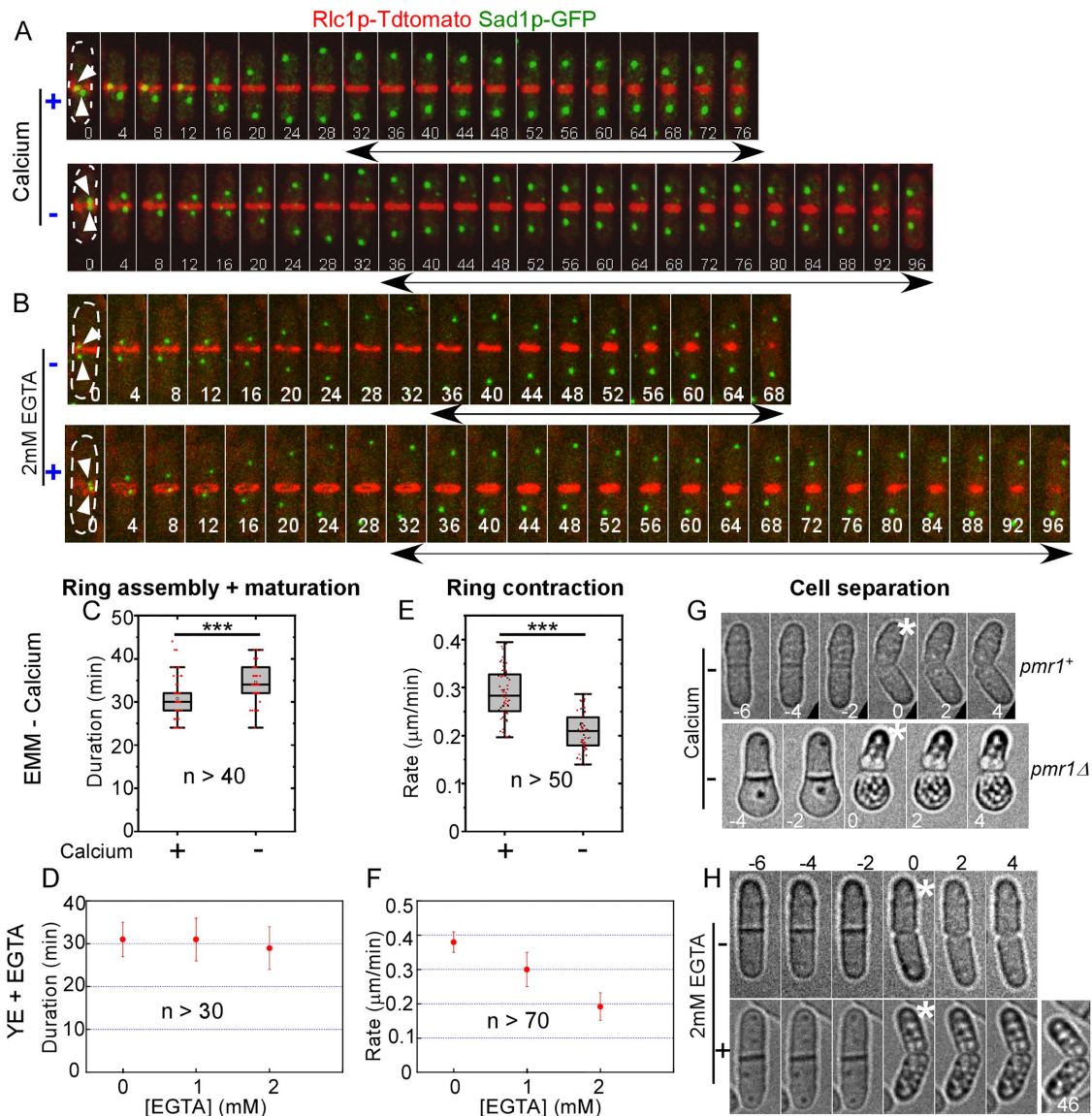


FIGURE 9: Temporary depletion of extracellular calcium slows down the contractile ring constriction and leads to daughter cell lysis. (A–F) Temporary depletion of extracellular calcium reduced the ring constriction rate, but it had only a minor effect on the ring assembly and maturation. (A, B) Temporary depletion of extracellular calcium slowed down the ring constriction. Time-lapse micrographs of dividing cells expressed both Sad1-GFP (green) and Rlc1p-tdTomato (red). Number: time in minutes after the separation of SPBs (arrowhead). Dashed line marks the outline of cells. (A) Cells in either regular EMM5s (top) or the calcium-free EMM5s media (bottom). (B) Cells in either YE5s (top) or YE5s plus 2 mM EGTA media (bottom). (C, D) Duration of the ring assembly plus maturation. The duration increased by 11% ($p < 0.001$) in the calcium-free EMM media (C), but it did not change significantly in the presence of EGTA. (E, F) The ring constriction rates. The rate decreased by 28% ($p < 0.001$) in the calcium-free EMM medium, E. (G, H) Temporary depletion of extracellular calcium increased the frequency of cell lysis among the daughter cells. Time-lapse micrographs of separating cells. Number: time in minutes after the cell separation. (G) The wild-type (top) or *pmr1* Δ (bottom) cells in the calcium-free EMM5s media (bottom). Although the wild-type cells ($n > 100$) did not lyse during the separation, $38 \pm 9\%$ of the mutant cells lysed (asterisk; $n = 60$). (H) The wild-type cells in either YE5s (top) or YE5s plus 2 mM EGTA (bottom). About 35% ($n = 103$) of daughter cells lysed after separation in the presence of EGTA. Data are pooled from two biological repeats. *** $p < 0.001$.

fluorescence signal inside the cells. The peaks or local maxima are detected by calculating the derivative at each point and identifying the points corresponding to the inversion of the derivatives from positive to negative. The locations and average fluorescence intensity values of individual peaks are then recorded. The video processing and analysis were performed using MATLAB (Mathworks, MA).

To measure the rate of contractile ring closure, we determined the duration of the ring closure by analyzing the fluorescence kymograph of the contractile ring. The closure rate was then calculated by dividing the initial circumference of the ring before the constriction by the duration. We used Image J (NIH) and custom-made macros for all the image analyses. The images were first corrected for X–Y drift using the ImageJ StackReg

plug-in (Thevenaz *et al.*, 1998) if necessary. Most plots were made with Kaleidagraph (Synergy, PA) except for the 3D plots, which were made with OriginLab (OriginLab, MA). The figures were made with Canvas (ACDSee Systems).

ACKNOWLEDGMENTS

The authors thank Debatrayee Sinha, Mamata Malla, Zachary Kreais, and Somaiyeh Khoubafarin for their technical help. They would also like to thank their colleagues at the University of Toledo, Song-Tao Liu, William Taylor, and Rick Komuniecki, for suggestions. They thank Dimitris Vavylonis (Lehigh University) and Ann Miller (University of Michigan) for thoughtful discussions. This work has been supported by the University of Toledo startup fund (QC), NIH R15GM134496 (QC) and the DeArce-Koch Memorial Fund (QC) and University of Toledo Undergraduate Summer Research and Creative Activities Program (OS).

REFERENCES

- Abenza JF, Couturier E, Dodgson J, Dickmann J, Chessel A, Dumais J, Salas REC (2015). Wall mechanics and exocytosis define the shape of growth domains in fission yeast. *Nat Commun* 6, 8400.
- Arnold JM (1975). Effect of calcium in cytokinesis as demonstrated with ionophore A23187. *Cytobiologie* 11, 1–9.
- Atilgan E, Magidson V, Khodjakov A, Chang F (2015). Morphogenesis of the fission yeast cell through cell wall expansion. *Curr Biol* 25, 2150–2157.
- Bahler J, Wu JQ, Longtine MS, Shah NG, McKenzie A 3rd, Steever AB, Wach A, Philippsen P, Pringle JR (1998). Heterologous modules for efficient and versatile PCR-based gene targeting in *Schizosaccharomyces pombe*. *Yeast* 14, 943–951.
- Balasubramanian MK, McCollum D, Chang L, Wong KC, Naqvi NI, He X, Sazer S, Gould KL (1998). Isolation and characterization of new fission yeast cytokinesis mutants. *Genetics* 149, 1265–1275.
- Batiza AF, Schulz T, Masson PH (1996). Yeast respond to hypotonic shock with a calcium pulse. *J Biol Chem* 271, 23357–23362.
- Cadou A, Couturier A, Le Goff C, Xie L, Paulson JR, Le Goff X (2013). The Kin1 kinase and the calcineurin phosphatase cooperate to link actin ring assembly and septum synthesis in fission yeast. *Biol Cell* 105, 129–148.
- Carbo N, Tarkowski N, Ipina EP, Dawson SP, Aguilar PS (2017). Sexual pheromone modulates the frequency of cytosolic Ca²⁺ bursts in *Saccharomyces cerevisiae*. *Mol Biol Cell* 28, 501–510.
- Chan CM, Aw JT, Webb SE, Miller AL (2016). SOCE proteins, STIM1 and Orai1, are localized to the cleavage furrow during cytokinesis of the first and second cell division cycles in zebrafish embryos. *Zygote* 24, 880–889.
- Chan CM, Chen Y, Hung TS, Miller AL, Shipley AM, Webb SE (2015). Inhibition of SOCE disrupts cytokinesis in zebrafish embryos via inhibition of cleavage furrow deepening. *Int J Dev Biol* 59, 289–301.
- Chang DC, Meng C (1995). A localized elevation of cytosolic free calcium is associated with cytokinesis in the zebrafish embryo. *J Cell Biol* 131, 1539–1545.
- Chang F, Drubin D, Nurse P (1997). *cdc12p*, a protein required for cytokinesis in fission yeast, is a component of the cell division ring and interacts with profilin. *J Cell Biol* 137, 169–182.
- Chen Q, Pollard TD (2011). Actin filament severing by cofilin is more important for assembly than constriction of the cytokinetic contractile ring. *J Cell Biol* 195, 485–498.
- Chen Q, Pollard TD (2013). Actin filament severing by cofilin dismantles actin patches and produces mother filaments for new patches. *Curr Biol* 23, 1154–1162.
- Chen TW, Wardill TJ, Sun Y, Pulver SR, Renninger SL, Baohan A, Schreiter ER, Kerr RA, Orger MB, Jayaraman V, *et al.* (2013). Ultrasensitive fluorescent proteins for imaging neuronal activity. *Nature* 499, 295–300.
- Clapham DE (2007). Calcium signaling. *Cell* 131, 1047–1058.
- Cortes JC, Ishiguro J, Duran A, Ribas JC (2002). Localization of the (1,3) beta-D-glucan synthase catalytic subunit homologue Bgs1p/Cps1p from fission yeast suggests that it is involved in septation, polarized growth, mating, spore wall formation and spore germination. *J Cell Sci* 115, 4081–4096.
- Cortes JC, Katoh-Fukui R, Moto K, Ribas JC, Ishiguro J (2004). *Schizosaccharomyces pombe* Pmr1p is essential for cell wall integrity and is required for polarized cell growth and cytokinesis. *Eukaryot Cell* 3, 1124–1135.
- Cortes JC, Sato M, Munoz J, Moreno MB, Clemente-Ramos JA, Ramos M, Okada H, Osumi M, Duran A, Ribas JC (2012). Fission yeast Ags1 confers the essential septum strength needed for safe gradual cell abscission. *J Cell Biol* 198, 637–656.
- Courtemanche N, Pollard TD, Chen Q (2016). Avoiding artefacts when counting polymerized actin in live cells with LifeAct fused to fluorescent proteins. *Nat Cell Biol* 18, 676–683.
- Craig R, Smith R, Kendrick-Jones J (1983). Light-chain phosphorylation controls the conformation of vertebrate non-muscle and smooth muscle myosin molecules. *Nature* 302, 436–439.
- Deng L, Sugiura R, Takeuchi M, Suzuki M, Ebina H, Takami T, Koike A, Iba S, Kuno T (2006). Real-time monitoring of calcineurin activity in living cells: evidence for two distinct Ca²⁺-dependent pathways in fission yeast. *Mol Biol Cell* 17, 4790–4800.
- Denis V, Cyert MS (2002). Internal Ca²⁺ release in yeast is triggered by hypertonic shock and mediated by a TRP channel homologue. *J Cell Biol* 156, 29–34.
- Fluck RA, Miller AL, Jaffe LF (1991). Slow calcium waves accompany cytokinesis in medaka fish eggs. *J Cell Biol* 115, 1259–1265.
- Garcia Cortes JC, Ramos M, Osumi M, Perez P, Ribas JC (2016). The cell biology of fission yeast septation. *Microbiol Mol Biol Rev* 80, 779–791.
- Jaffe LF, Creton R (1998). On the conservation of calcium wave speeds. *Cell Calcium* 24, 1–8.
- Laplante C, Berro J, Karatekin E, Hernandez-Leyva A, Lee R, Pollard TD (2015). Three myosins contribute uniquely to the assembly and constriction of the fission yeast cytokinetic contractile ring. *Curr Biol* 25, 1955–1965.
- Liu J, Wang H, McCollum D, Balasubramanian MK (1999). Drc1p/Cps1p, a 1,3-beta-glucan synthase subunit, is essential for division septum assembly in *Schizosaccharomyces pombe*. *Genetics* 153, 1193–1203.
- Ma Y, Sugiura R, Koike A, Ebina H, Sio SO, Kuno T (2011). Transient receptor potential (TRP) and Cch1–Yam8 channels play key roles in the regulation of cytoplasmic Ca²⁺ in fission yeast. *PLoS One* 6, e22421.
- Martin-Garcia R, Arribas V, Coll PM, Pinar M, Viana RA, Rincon SA, Correa-Bordes J, Ribas JC, Perez P (2018). Paxillin-mediated recruitment of calcineurin to the contractile ring is required for the correct progression of cytokinesis in fission yeast. *Cell Rep* 25, 772–783.e774.
- Miller AL, Fluck RA, McLaughlin JA, Jaffe LF (1993). Calcium buffer injections inhibit cytokinesis in *Xenopus* eggs. *J Cell Sci* 106 (Pt 2), 523–534.
- Mishra M, Kashiwazaki J, Takagi T, Srinivasan R, Huang Y, Balasubramanian MK, Mabuchi I (2013). In vitro contraction of cytokinetic ring depends on myosin II but not on actin dynamics. *Nat Cell Biol* 15, 853–859.
- Mitchison JM, Nurse P (1985). Growth in cell length in the fission yeast *Schizosaccharomyces pombe*. *J Cell Sci* 75, 357–376.
- Moser MJ, Flory MR, Davis TN (1997). Calmodulin localizes to the spindle pole body of *Schizosaccharomyces pombe* and performs an essential function in chromosome segregation. *J Cell Sci* 110 (Pt 15), 1805–1812.
- Muñoz J, Cortés JCG, Sipiczki M, Ramos M, Clemente-Ramos JA, Moreno MB, Martins IM, Pérez P, Ribas JC (2013). Extracellular cell wall beta(1,3) glucan is required to couple septation to actomyosin ring contraction. *J Cell Biol* 203, 265–282.
- Nagai T, Sawano A, Park ES, Miyawaki A (2001). Circularly permuted green fluorescent proteins engineered to sense Ca²⁺. *Proc Natl Acad Sci USA* 98, 3197–3202.
- Nakai J, Ohkura M, Imoto K (2001). A high signal-to-noise Ca²⁺ probe composed of a single green fluorescent protein. *Nat Biotechnol* 19, 137–141.
- Nishimura J, Khalil RA, Drenth JP, van Breemen C (1990). Evidence for increased myofilament Ca²⁺ sensitivity in norepinephrine-activated vascular smooth muscle. *Am J Physiol* 259, H2–H8.
- Noguchi T, Mabuchi I (2002). Localized calcium signals along the cleavage furrow of the *Xenopus* egg are not involved in cytokinesis. *Mol Biol Cell* 13, 1263–1273.
- Pollard TD, Wu JQ (2010). Understanding cytokinesis: lessons from fission yeast. *Nat Rev* 11, 149–155.
- Proctor SA, Minc N, Boudaoud A, Chang F (2012). Contributions of turgor pressure, the contractile ring, and septum assembly to forces in cytokinesis in fission yeast. *Curr Biol* 22, 1601–1608.
- Scholey JM, Taylor KA, Kendrick-Jones J (1980). Regulation of non-muscle myosin assembly by calmodulin-dependent light chain kinase. *Nature* 287, 233–235.
- Sipiczki M (2007). Splitting of the fission yeast septum. *FEMS Yeast Res* 7, 761–770.

- Snow P, Nuccitelli R (1993). Calcium buffer injections delay cleavage in *Xenopus laevis* blastomeres. *J Cell Biol* 122, 387–394.
- Takeda T, Yamamoto M (1987). Analysis and in vivo disruption of the gene coding for calmodulin in *Schizosaccharomyces pombe*. *Proc Natl Acad Sci USA* 84, 3580–3584.
- Thevenaz P, Ruttimann UE, Unser M (1998). A pyramid approach to subpixel registration based on intensity. *IEEE Trans Image Process* 7, 27–41.
- Tian L, Hires SA, Mao T, Huber D, Chiappe ME, Chalasani SH, Petreanu L, Akerboom J, McKinney SA, Schreiter ER, et al. (2009). Imaging neural activity in worms, flies and mice with improved GCaMP calcium indicators. *Nat Methods* 6, 875–881.
- Wu JQ, Kuhn JR, Kovar DR, Pollard TD (2003). Spatial and temporal pathway for assembly and constriction of the contractile ring in fission yeast cytokinesis. *Dev Cell* 5, 723–734.
- Yoshida T, Toda T, Yanagida M (1994). A calcineurin-like gene *ppb1+* in fission yeast: mutant defects in cytokinesis, cell polarity, mating and spindle pole body positioning. *J Cell Sci* 107 (Pt 7), 1725–1735.